Deformation Instability of Light Alloys under Dynamic Compression

Vladimir V. Skripnyak[1, a)], Natalia V. Skripnyak[1, b)], Alexander E. Kiryushkin[1,c)], and Vladimir A. Skripnyak[1,d)]

[1]*National Research Tomsk State University, 36 Lenin Avenue, Tomsk, Russia, 634050*

[a)] Corresponding author: skrp2012@yandex.ru
[b)] natali.skrp@mail.ru,
[c)] sashakir94@mail.ru,
[d)] skrp2006@yandex.ru

Abstract. The instability formation of plastic deformation of aluminum and magnesium alloys under tension or compression at strain rates from 0.1 up to 1000 s^{-1} was investigated by experimental tests and numerical simulation. The experimental results of the study of the processes of development of plastic deformations in samples of AMg3, AMg6 and MA2-1 alloys under uniaxial tension and uniaxial compression were obtained during tests on the Instron VHS 40/50-20 servo hydraulic stand. It was found that the studied alloys exhibit asymmetry in the true stress versus true strain curves under uniaxial compression or tension. The ratio values of plastic flow stress under uniaxial tension and compression at the same initial temperatures and equivalent plastic strains depends on the strain rate. Predictions of macroscopic instability of plastic flow of the studied alloys in accordance with the Considere criterion are consistent with the obtained experimental data. It is shown that the onset of macroscopic instability of plastic flow in aluminum and magnesium alloys occurs at various equivalent plastic deformations under conditions of high strain rates uniaxial compression or tension. At a strain rates higher than 100 s^{-1} Strain localization in the magnesium alloy MA2-1 starts under compression at essentially low values of equivalent plastic strain than at tension with similar strain rates. It was established that during uniaxial compression of aluminum alloys AMg3 and AMg6 in the range of deformation rates from 0.1 to 1000 s^{-1}, the instability of the macroscopic plastic flow process does not occur.

INTRODUCTION

Application extensions of dynamic forming technologies for rolled aluminum and magnesium alloys without preheating for the manufacture of structural elements for aerospace, automotive required an increasing in the accuracy of describing the patterns of plastic deformation of alloys in the computer designing of pressing process modes [1, 2]. In this regard, an important task is to obtain information on the mechanical behavior of structural light alloys in a wide range of loading conditions, including dynamic effects.

Aluminum and magnesium alloys have similar melting points, but belong to different isomechanical groups of materials [3].

Increasing the accuracy of predicting the formability of light alloys under complex loading conditions is associated with taking into account the difference in resistance to plastic deformation under tension and compression [4-6].

One of the important aspects of describing the mechanical behavior of deformable magnesium alloys under high-speed deformation of products is predicting the localization of plastic deformation and the development of damage. Studies have shown that both the equivalent strain rate and the stress state triaxiality parameter ($\eta = -p/\sigma_{eq}$, where p is the pressure and σ_{eq} is the equivalent von Mises stress) have a significant effect on the conditions of damage and fracture of magnesium and aluminum alloys during dynamic punching [7, 8].

The aim of this work was to study the plastic flow instability of AMg3, AMg6 and MA2-1 alloys under tension and compression in strain rate range from 0.1 to 1000 s^{-1}.

The results of experimental and theoretical studies of the mechanical behavior of magnesium and aluminum alloys at high strain rates obtained in the work complement the data obtained earlier.

MATERIALS AND TESTING METHOD

Tension and compression tests at various constant strain rates were carried out using an Instron VHS 40/50-20 high-speed test bench (Instron Corporation, High Wycombe, UK) with a 50 kN load cell.

The dog bone shape specimens with initial gauge length of 20 ± 0.1 mm and thickness of 1.05 ± 0.05 mm were used for tension tests in accordance with the requirements of standards ISO 26203-2-2011, ASTM E8/E8M, GOST 1497-84.

The alloy's resistance to uniaxial compression of alloys in accordance of ASTM E9.09 and GOST 25.503-97 standards were obtained at strain rates of 0.1, 1, 100, 1000 1/s.

The cylindrical specimens were used for uniaxial compression tests. The samples had a diameter-to-height ratio of 1.The ends of the specimens were ground and polished after being cut from the rod. The specimens before testing are shown in Fig.1.

(a) (b) (c)

FIGURE 1. Photograph of samples before testing (a) MA2-1, (b) AMg6, (c) AMg3

All samples were cut out from cylindrical rolled bars alloys using electrical erosion method. Compression testing of the cylindrical specimens on the VHS 40/50-20 rig yielded data on specimen loading forces and changing of their height over time. The tests were performed in the velocity control mode at the initial values of the compression velocity of 0.002 ± 0.00001, 2 ± 0.01, and 10 ± 0.02 m/s.

Reducing the coefficient of friction between the samples and punch was achieving by IPF ER-3 lubricant (OOO Gazpromneft - lubricant, Moscow, Russia) oil lubricant.

The initial temperature of the sample was measured using an ADA TemPro 900 infrared pyrometer with a response time of 0.5 s and an accuracy of 1.5 K.

Samples for compression tests were made from round rolled products of industrial alloys AMg3, AMg6, MA-2. AMg3 (Al 1530), AMg6 (Al 1560) polycrystalline aluminum alloys were manufacturing accordingly of GOST 4784–97.

The AMg3 had a chemical composition in wt. %: 3.42 % Mg, 0.06 % Mn, 0.4 % Fe, 0.31 % Si, 0.05 % Cu, 0.203% Zn, 0.0843 %Ti, 0,086 % Cu, Al is the balance.

The AMg6 had a chemical composition in wt. %: 6,124 % Mg, 5.977 % Mn, 0,351 % Fe, 0,610 % Si, 0,183 % Zn, 0,083 % Ti, 0.076 % Cu, Al is the balance.

The MA2-1 alloy had a chemical composition in wt. %: 93.7% Mg, 4.36% Al, 1.34% Zn and 0.39% Mn, and a mass density of 1.79 ± 0.02 g/cm^3. The alloy was in a polycrystalline state with an average grain size of ~ 40 μm.

At the room temperature AMg3 alloy has the yield strength $\sigma_{0.2}$ of ~80 MPa and the uniaxial tensile strength σ_{UTS} of 175 MPa under quasi static tension. The Young's modulus E is 71 GPa, the shear modulus is 26.69 GPa, and Poisson's ratio is ν = 0.33, specific heat capacity C_p= 880 J/(kg•K), Taylor-Quinney coefficient β ≈ 0.9.

At the room temperature AMg6 alloy has the yield strength of ~190 MPa and a tensile strength of 355 MPa. The Young's modulus is 71 GPa, the shear modulus is 26.7 GPa, and Poisson's ratio is ν = 0.33, specific heat capacity C_p= 992 J/(kg•K), Taylor-Quinney coefficient $\beta \approx 0.9$.

Industrial rolled polycrystalline MA2-1 alloy have the chemical composition (wt. %): 93.7 % Mg, 4.36 % Al, 1.34 % Zn and 0.39 % Mn, and the average grain size was equal to 80 ± 10 μm.

The mass density of MA2-1 alloy was 1.79 g/cm^3 under quasi-static loads at a temperature of 295 K, the alloy with an average grain size of 40 μm had the yield strength of $\sigma_{0.2}$ = 150 MPa, tensile strength σ_{UTS} = 260–280 MPa, elongation before failure δ ~ 5…12%.

At the room temperature MA2-1 alloy have the shear modulus μ = 16.5 GPa, the Young's modulus E = 44.55 GPa, the Poisson's ratio υ = 0.35, the quasi static yield strength $\sigma_{0.2}$ = 150 ±5 MPa, the tensile strength σ_{UTS} = 250±10 MPa, the linear thermal expansion coefficient 26•10^{-6} K^{-1}, specific heat capacity C_p= 1088.5 J/(kg•K), and Taylor-Quinney coefficient $\beta \approx 0.4…0.6$ [9].

It should be noted that the melting temperatures T_m of AMg3 (858 K…928 K), AMg6 (883 K …923 K) and MA2-1 (903 K…923 K) alloys are close. Therefore, the homologous temperature T/T_m corresponding to room temperature, is approximately the same for all the alloys studied in this work tests.

The tensile force and displacement of specimens were recorded at high temporal resolution up to complete fracture of the specimen using the VHS 40/50-20. True stress versus true strain curves were determined using obtained tensile force and displacement of alloys specimens under tension and compression tests in in accordance of standards ISO 26203-2-2011, ASTM E8/E8M and recommendation of [10].

DEFORMATION INSTABILITY CRITERION FOR LIGHT ALLOYS UNDER DYNAMIC COMPRESSION

The Considere criterion [11] was used as a criterion for the origin of plastic deformation instability leading to the formation of macro localization bands

$$\frac{\partial \sigma_s}{\partial \varepsilon_{\text{eq}}^p} + \frac{\partial \sigma_s}{\partial \dot{\varepsilon}_{\text{eq}}^p}\frac{\partial \dot{\varepsilon}_{\text{eq}}^p}{\partial \varepsilon_{\text{eq}}^p} + \frac{\partial \sigma_s}{\partial T}\frac{\partial T}{\partial \varepsilon_{\text{eq}}^p} + \frac{\partial \sigma_s}{\partial g^*}\partial \frac{g^*}{\partial \varepsilon_{\text{eq}}^p} = \sigma_s \quad (1)$$

where σ_{eq}= $[(3/2)\sigma_{ij}\ \sigma_{ij} - 0.5\ \sigma^2_{kk}]^{1/2}$, is the Mises equivalent stress, σ_{ij} are the stress tensor components, $\varepsilon_{eq}^p = [(2/3)\varepsilon_{ij}^p \varepsilon_{ij}^p]^{1/2}$ is equivalent plastic strain, T is the temperature in K, g* is the damage parameter of the alloy.

Criterion (1) takes the form (2) under loading at a high constant strain rate, and absence of damage in the initial alloy state

$$\frac{\partial \sigma_s}{\partial \varepsilon_{\text{eq}}^p} = (1 - \frac{\partial \sigma_s}{\partial T}\frac{\beta}{\rho c_p})\sigma_s \quad (2)$$

where β is the Taylor – Quinney coefficient, ρ is the mass density, Cp is the specific heat capacity.

The temperature increment during plastic flow due to energy dissipation was determined in the adiabatic approximation [3]

$$T = T_0 + \int_0^{\varepsilon_{\text{eq}}^p} (\beta/\rho\ C_p)\ \sigma_{\text{eq}}\, d\, \varepsilon_{\text{eq}}^p, \quad (3)$$

where T_0 is the initial temperature, β is the Taylor-Quinney coefficient.

The flow stress of the alloy during damage development was described using the constitutive relation [12]

$$(\sigma_{\text{eq}}^2/\ \sigma_s^c \sigma_s^t) + 2q_1\, g^* \cosh[-q_2\, p/(2\sqrt{\sigma_s^c \sigma_s^t})] + (1 - g^*)[3(\sigma_s^c - \sigma_s^t)/\sigma_s^c\ \sigma_s^t]p\text{-}1\text{-}(\ q_3(g^*)^2 = 0 \quad (4)$$

where σ^c_s is the yield strength under compression, σ^t_s is the yield strength under tension, p is the pressure, q_1, q_2 and q_3 are the model parameters, and g* is the material damage parameter.

Equation (4) can be reduced to the traditional Gurson-Tvergaard-Needleman form if the difference between σ^t_s and σ^c_s is negligible [8].

Needleman's damage kinetics equations can be used for determination changes of g* during plastic flow [7, 8, 13].

Experimental true stress versus true strain curves at various strain rates can be used for calibration of constitutive equations Zerilli-Armstrong (ZA) for aluminium and magnesium alloys. The variant of ZA constitutive equation for alloys with a face-centered cubic (FCC) lattice should be used for aluminum alloys [3, 8], and the variant of ZA equation for a subgroup of alloys with a hexagonal close-packed crystal lattice can be used for magnesium alloys [7, 14].

RESULTS AND DISCUSSION

Experimental true stress versus true strain obtained at tension and compression of AMg3, AMg6 and MA2-1 alloys under strain rates of 0.1, 100, and 1000 s^{-1} are shown in Fig. 2.

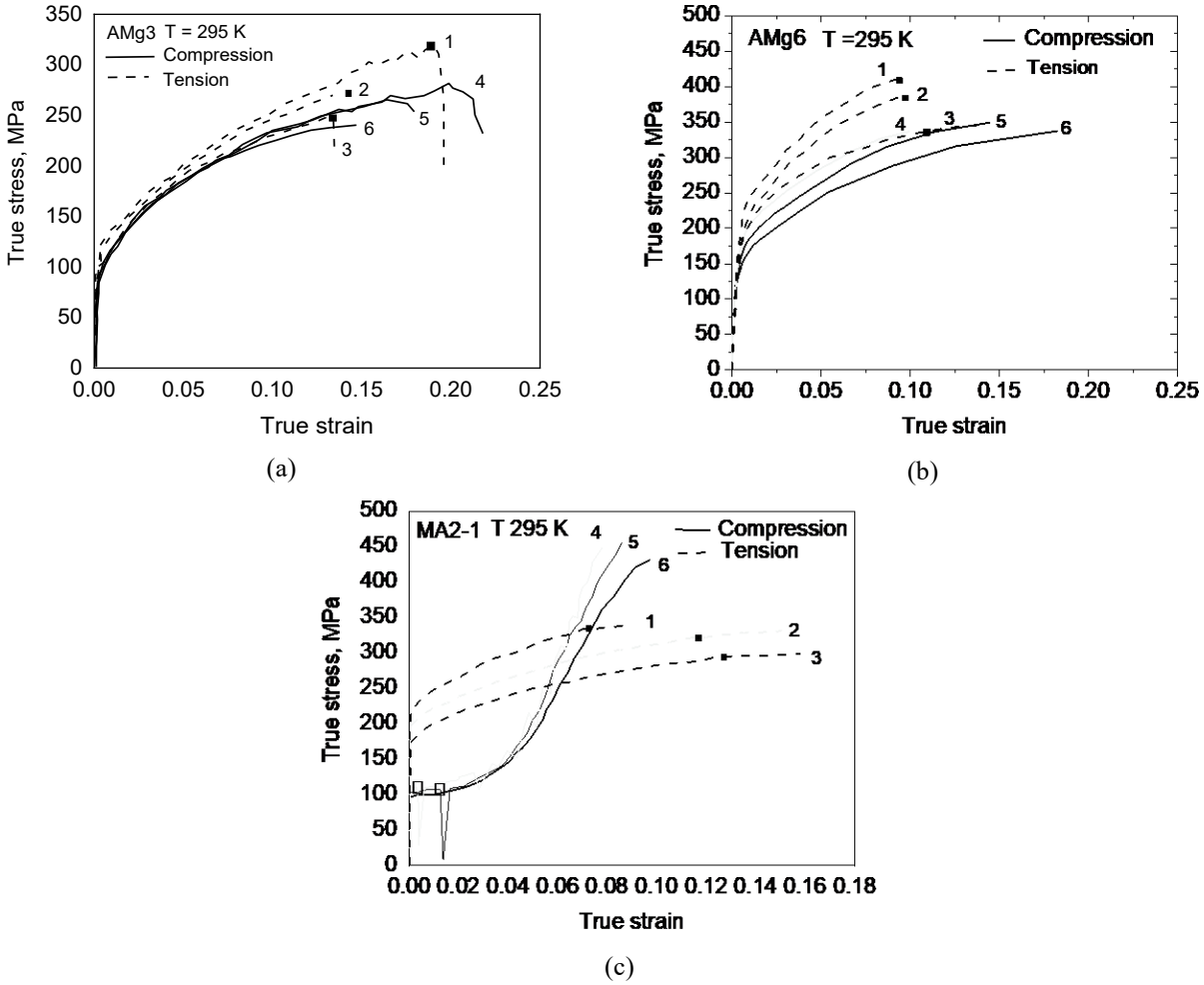

FIGURE 2. Experimental true stress versus true strain of AMg3 (a) curves 1, 4 at strain rate of 1000 s-1; curves 2, 5 at 100 s-1; curves 3, 6 at 0.1 s-1; AMg6 (b) , MA2-1 (c) . Initiation of localization bands shown by filled square symbols the under tension, and filled rhombic symbols under compression

The true stress – true strain curves under tension of AMg3 alloy at strain rates of 1000, 100, and 0.1 s-1 exhibit states that satisfy the plastic flow instability criterion (2). These conditions are shown on the curves by filled square symbols. The strain localization develops and specimen neck before failure formed when the equivalent plastic strain exceeds the critical values depending on strain rates and temperatures. Experimental results obtained during compression tests of the AMg3 alloy showed that the true stress – true strain curves do not contain states that satisfy criterion (2). These results are confirmed by an analysis of the strain state of the specimens after compression testing. Photographs of the specimens after testing are shown in Fig. 3(a), (b), (c).

Similar results were obtained when testing specimens of the stronger AMg6 aluminum alloy. Plastic flow instability occurred at the strain ~0.1 under uniaxial tension of AMg6 specimens, leading to the formation of a region of macro localized deformation before failure. However, under uniaxial compression in the strain rate range from 0.1 to 1000 s^{-1}, plastic flow instability did not occur. Photographs of the specimens without any signs of shear localization after testing are shown in Fig. 3(d), (e), (f).

Under uniaxial tension of the AMg6 alloy, the equivalent plastic strain at which instability occurred insignificantly decreased with increasing strain rate. The change in the conditions for the onset of plastic flow instability under uniaxial tension of AMg3 and AMg6 alloys is due to differences in the strain hardening patterns of the alloys at equivalent strain rates and temperatures. This is due to the effect on the strain hardening patterns of the higher magnesium mass concentration in the AMg6 alloy.

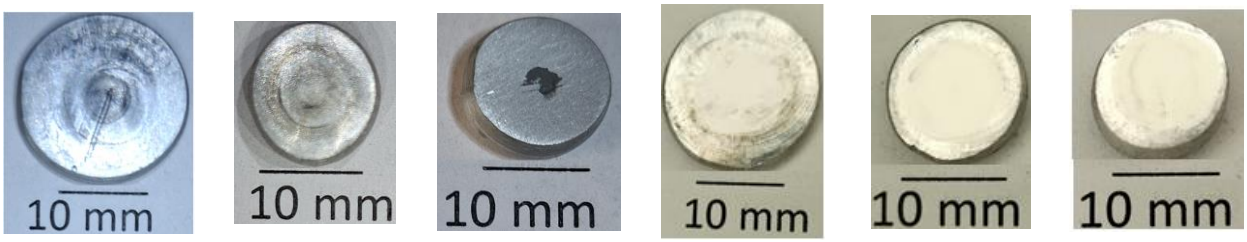

(a) (b) (c) (d) (e) (f)

FIGURE 3. Photographs of AMg3 samples after dynamic compression at strain rates of 1000 s^{-1} (a), 100 s^{-1} (b), 0.1 s^{-1} (c); of AMg6 samples after dynamic compression at strain rates of 1000 s^{-1} (d), 100 s^{-1} (e), 0.1 s^{-1} (f);

The true stress – true strain curves under tension of magnesium alloy at strain rates of 1000, 100, and 0.1 s^{-1} exhibit states that satisfy the plastic flow instability criterion (2). Tests were carried out on samples of the MA2-1 alloy under uniaxial tension or compression. The significant difference between the true stress and true strain curves under tension and compression, which can be seen in Fig. 2(c), was discussed earlier by Lei et al. [15]. The results obtained in the work showed that a significant difference in the patterns of strain hardening of magnesium alloy MA2-1 under compression and tension is maintained in a wide range of deformation rates from 0.1 to 1000 s^{-1}.

The plastic flow instability was discovered under uniaxial tension at all studied strain rates and under compression at strain rate above of the 100 s^{-1}. Photographs of the specimens after testing are shown in Fig. 4 (a), (b), (c). The specimens after testing with clear signs of shear localization shown in Fig. 4 (a), (b). The true stress vs true strain curves have oscillation caused by developing of local shearing of the material volume blocks. The stress relaxation starts correlates with the predictions of the occurrence of plastic flow instability based on criterion (2).

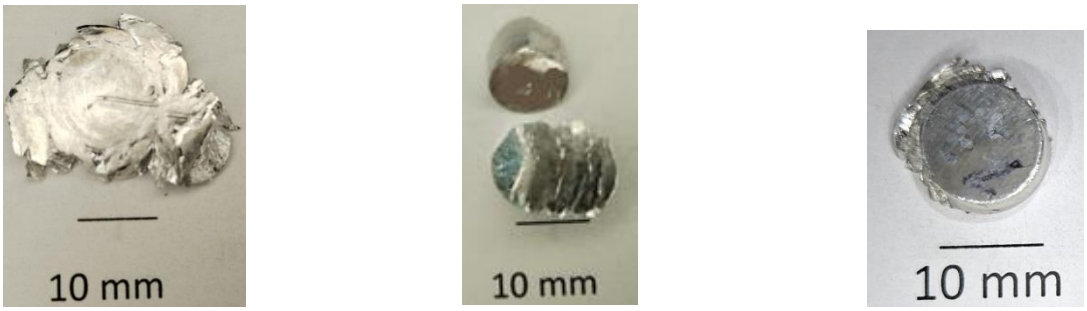

(a) (b) (c)

FIGURE 4. Photographs of MA2-1 alloy samples after dynamic compression at strain rates of 1000 s^{-1} (a), 100 s^{-1} (b), 0.1 s^{-1} (c)

It was noted that, under compression at strain rates below 10 s^{-1}, localized shear of the bulk material blocks does not occur in MA2-1 specimens with the of the indicated geometric characteristics used. As the strain rate increases, plastic flow instability repeatedly occurs in the parts of low deformed specimen. This results in the formation of multiple localized shears in the material. The formation of multiple shears is accompanied by the generation of audible signals in the form of crackling sounds, which correlates with the formation of specimen fragments, which can be seen Fig. 4 (a) and (b).

CONCLUSION

An experimental research of AMg3, AMg6, MA2-1 alloys mechanical response to uniaxial tension and compression at strain rates of 0.1, 100, and 1000 s^{-1} at room temperature were carried out.

1. It is shown that in cylindrical samples of aluminum alloys AMg3, AMg6 under uniaxial compression at the studied strain rates, instability of macroscopic plastic flow does not occur, accompanied by the formation of shear bands leading to the samples failure.
2. The true stress–strain curves of MA2-1 magnesium alloy under uniaxial tension and compression at strain rates of 0.1, 100, and 1000 s^{-1} at room temperature differ qualitatively. The magnesium alloy exhibits not only asymmetry in tensile and compressive yield strengths over a wide range of strain rates but also distinct strain hardening patterns. The asymmetry of resistance to plastic deformation under compression and tension over a wide range of strain rates must be taken into account in wide-range constitutive equations.

3. The experimental results confirm the need to use different constitutive equations for aluminum alloys belonging to the FCC isomechanical group of alloys and for magnesium alloys belonging to the HCP isomechanical subgroup of metallic materials.
4. 3. The emergences of instability plastic flow, recorded in experiments on uniaxial tension and compression of AMg3, AMg6, and MA2-1 alloy samples, correlate well with the predictions according to the Considere criterion at strain rates of 0.1, 100, and 1000 s^{-1} and at room temperature.

ACKNOWLEDGMENTS

The work was supported by the Russian Science Foundation: project 24-79-10103. The authors thank the Russian Science Foundation for research support.

REFERENCES

1. M.-S. Joun, M.K. Razali, C.-W. Jee, J.-B. Byun, M.-C. Kim, K.-M. Kim, A review of flow characterization of metallic materials in the cold forming temperature range and its major issues, Materials **15**, 2751 (2022). https://doi.org/10.3390/ma15082751
2. J. Yang, Z. Zhu, S. Han, Y. Gu, Z. Zhu, H.-D. Zhang, Evolution, limitations, advantages, and future challenges of magnesium alloys as materials for aerospace applications, J. Alloy. Compd. **1008**, 176707 (2024). https://doi.org/10.1016/j.jallcom.2024.176707
3. Frost, H.J.; Ashby, M.F. *Deformation-Mechanism Maps* (Pergamon Press: Oxford, UK, 1982). 166 p.
4. P.D. Barros, M.C. Oliveira, L.F. Menezes, Study on the effect of tension-compression asymmetry on the cylindrical cup forming of an AA2090-T3 alloy, Int. J. Solids Struct. **151**, 135-144 (2018). https://doi.org/10.1016/j.ijsolstr.2017.06.034
5. L. Chen, J. Zhang, H. Zhang, Anisotropic yield criterion for metals exhibiting tension–compression asymmetry, AAMM **13**, 701-723 (2021). https://doi.org/10.4208/aamm.oa-2019-0328
6. F. Xiuli, S. Qihang, W. Hui, P. Yongzhi, EFFECT Analysis of high strain rate and anisotropy on tension **-** compression asymmetry of aluminum alloy 7050, Trans. Nanjing Univ. Aeronaut. **37**, 376-384 (2020). https://doi.org/10.16356/j.1005-1120.2020.03.004
7. V. V. Skripnyak, N. V. Skripnyak, O. N. Zagorodkin, V. A. Skripnyak, Ductile fracture of Mg–3Al–1Zn alloy under dynamic loads, Vestnik Tomskogo gosudarstvennogo universiteta. Matematika i mekhanika – Tomsk State University Journal of Mathematics and Mechanics **95**, 164–179 (2025). https://doi.org/10.17223/19988621/95/14
8. V.A. Skripnyak, M.O. Chirkov, V.V. Skripnyak, Mechanical behavior of aluminum alloy 1520 under tension in the range of strain rates from 10^{-1} to 10^{3} s^{-1}. Vestnik Tomskogo gosudarstvennogo universiteta. Matematika i mekhanika – Tomsk State University Journal of Mathematics and Mechanics **86**, 120–135 (2023). https://doi.org/10.17223/19988621/86/9
9. N. A. Ozdur, S. C. Ermana, R. Seghir, L. Stainier, C.C. Aydıner, A thermomechanical investigation of textured magnesium in an effort to validate crystalplasticity simulations, Procedia Structural Integrity IWPDF 2023, 61, 277–284 (2024) Procedia Structural Integrity **61**. pp. 277–284. https://doi.org/10.1016/j.prostr.2024.06.035
10. J.K. Holmen, B. H. Frodal, H. Bjørn, O.S. Hopperstad, T. Børvik, Strength differential effect in age hardened aluminum alloys. Int. J. Plast, **99** S0749-6419(17)30321-2 (2017). doi:10.1016/j.ijplas.2017.09.004
11. I.S. Yasnikov, A. Vinogradov, Y. Estrin, Revisiting the Considère criterion from the viewpoint of dislocation theory fundamentals, Scr. Mater. **76**, 37–40 (2014). https://doi.org/10.1016/j.scriptamat.2013.12.009
12. X. Zhu,·Y. Lei, H. Wan,· S. Li, G. Dui Constitutive modeling of porosity and grain size effects on superelasticity of porous nanocrystalline NiTi shape memory alloy, Acta Mechanica. **234**, 6499 – 6513 (2023). https://doi.org /10.1007/s00707-023-03721-0
13. A. Needleman, V. Tvergaard, Analyses of plastic flow localization in metals, Appl. Mech. Rev. **45**, S3–S18 (1992). https://doi.org/10.1115/1.3121390
14. C.Y. Gao, L.C. Zhang, H.X. Yan, A new constitutive model for HCP metals, Mater. Sci. Eng. A **528** 4445–4452 (2011). https://doi.org/10.1016/j.msea.2011.02.053
15. Y. Lei, M. Zhan, H. Xin, L. Ma, Y. Yuan, H. Zhang, Z. Zheng, Comparison of the strain rate sensitivity in AZ31 and WE43 magnesium alloys under different loading conditions, Crystals, **13**, 554 (2023). https://doi.org/10.3390/cryst13040554